J Mater Sci (2009) 44:1045–1053
DOI 10.1007/s10853-008-3211-z

Structural, mechanical, and tribological properties of AISI 304 and AISI 316L steels submitted to nitrogen–carbon glow discharge

F. C. Nascimento · C. M. Lepienski · C. E. Foerster · A. Assmann · S. L. R. da Silva · C. J. de M. Siqueira · A. L. Chinelatto

Received: 18 September 2008 / Accepted: 19 December 2008 / Published online: 13 January 2009

Abstract Glow discharge (GD) nitrocarburizing, at low-carbon content and different working temperatures, was performed on AISI 316L and AISI 304 stainless steels. Structural compositions were studied by X-ray diffraction. Instrumented indentation and conventional Vickers method allowed hardness profiles to be determined. Tribological behavior was studied by means of reciprocating sliding and nanoscratch tests. After nitrocarburizing, both steels showed similar embedded nitride and carbide formations. The layer formed by GD in nitrogen–carbon atmosphere is thicker than those consisting solely of nitrogen particularly for AISI 316L. At working temperatures higher than 400 °C, roughness increased and wear was limited to asperity compaction. Wear mechanisms were similar in both steels. However, wear was reduced by up to a factor of 5 in treated steels. No difference in elastic surface recovery was observed after nitrocarburizing in either steel.

F. C. Nascimento · C. E. Foerster · A. Assmann · S. L. R. da Silva
Depto. de Física, UEPG, 84030-900 Ponta Grossa, PR, Brazil

C. M. Lepienski (✉)
Depto. de Física, UFPR, CP 19044, 81531-990 Curitiba, PR, Brazil
e-mail: lepiensm@fisica.ufpr.br

C. J. de M. Siqueira
Depto. de Eng. Mecânica, UFPR, CP 19011, 81531-990 Curitiba, PR, Brazil

A. L. Chinelatto
Depto. de Eng. de Materiais, UEPG, 84030-900, 81531-990 Ponta Grossa, PR, Brazil

Introduction

Tailoring of metallic surfaces, in order to improve mechanical properties and tribological and corrosive resistance, is important in various engineering areas. Common metal alloys employed in these productive segments are AISI 304 and AISI 316L stainless steels. The above-said alloys are submitted to surface treatments (such as nitriding) in order to improve wear resistance. However, if these treatments are performed at temperatures exceeding 420 °C, chromium depletion and a decrease in corrosion resistance occur.

Ion nitriding, including glow discharge (GD), plasma immersion implantation (PI3), and ion implantation, has been used to modify the surface properties of steels [1–14]. At working temperatures lower than 400 °C, expanded austenite (γ_N, nitrogen in solid solution) is formed, whereas at higher temperatures, γ'-Fe_4N, ε-$Fe_{2+x}N$, and CrN phases are observed. The thickness of the modified surface is more dependent on temperature than nitriding time. Nitriding atmosphere composition (nitrogen–hydrogen content) can influence precipitate composition and thickness; however, its effects on hardness values are insignificant.

Recently certain authors reported on the use of mixed nitrogen–carbon atmospheres in GD and PI3 processes for steels [15–20]. Carbon content of these mixed atmospheres ranged from poor to rich, based on C_2H_2 or CH_4 gases. As a result of the use of carbon in nitriding atmospheres, modified layers are thicker than those obtained by the use of traditional nitrogen–hydrogen atmospheres at similar working temperatures. Although a carbon peak at near surface region is present, carbon presence is observed after the nitrogen profile. Some authors [16–18] also reported a slightly increase in corrosion resistance as a result of using a mixed nitrogen–carbon atmosphere. However, this is an

unexpected result because it is well known that if chromium carbide or nitrides are present in the modified surface, the corrosion resistance will be reduced.

This article reports on the influence of carbon presence in GD nitriding atmospheres on surface structure and mechanical and tribological properties of AISI 304 and AISI 316L steels. Considering the deleterious effect of carbon on corrosion resistance, the content of CH_4 in the nitriding atmosphere was 2%. Substrate temperatures were ranged from 400 to 500 °C.

Experimental procedure

Commercial stainless steel sheets of AISI 304 (Ni 8.63 wt%; Cr 16.04 wt%, C 0.047 wt%, Si 0.48 wt%, Mn 1.37 wt%, S 0.005 wt%, P 0.029 wt% and Fe being the balance) and AISI 316L (Ni 11.02 wt%; Cr 14.90 wt%, C 0.032 wt%, Si 0.53 wt%, Mn 1.42 wt%, S 0.005 wt%, P 0.043 wt%, Mo 1.86 wt% and Fe being the balance) were cut into pieces of size 2 cm × 2 cm × 5 mm. These pieces were mechanically polished up to ¼ μm using diamond paste in order to obtain a mirror finish and, subsequently, cleaned in an ultrasound bath. They were not homogenized, and grain sizes of both steels were in the order of 20 to 30 μm.

The DC GD was performed with a gas mixture of 98:2—N_2:CH_4 at 450 Pa with a prior H_2 sputtering at 100 °C for 2 h. The plasma current ranged from 200 to 300 mA resulting in sample ensembles with substrate temperatures of 400, 450, and 500 °C. The temperature was controlled by monitoring a backside thermocouple and adjusting the plasma current as needed. All samples were nitrocarburized for 4 h.

The phases were identified by X-ray diffraction data (CuK_α, λ= 1.5406 Å) collected between $20° \leq 2\theta \leq 80°$ at room temperature The step scan mode was with a width of 2θ—0.02 and a 5 s counting time. Near surface regions were studied on the basis of glancing-incidence X-ray analyses at $\alpha = 2$ and 5°. Crystalline planes were indexed using Joint Committee on Powder Diffraction Standards (JCPDS) cards [21] and the Inorganic Crystal Structure Database (ICSD). Structural characterization was performed by means of the Rietveld method [22, 23] with the code Fullprof, using a pseudo-Voigt function [24].

Hardness profiles at shallow depths were obtained by instrumented indentation following the Oliver and Pharr method [25]. The indenter was a Berkovich type, and the applied loads were up to 400 mN. For deeper regions, hardness profiles were obtained by conventional Vickers hardness tests, and the applied loads were up to 5 N. Roughness was analyzed from profilometry, performed by an instrumented indentation device, with loads approximately 300 μN. Nanoscratch tests were performed with a diamond Berkovich tip in ramping loads from 0 to 400 mN following the tip edge direction. The lengths of the nanoscratches were up to 1 mm. Tip penetration profiles were monitored before, during, and after scratching. Elastic recovery was determined taking into account original surface topography.

Wear tests were performed under severely dry conditions at room temperature and at 50% humidity. The counter body was a WC (Co) ball ($\phi = 6$ mm) with a load of 5.0 N. The sliding velocity was 1 cm/s, with a half-amplitude of 1.0 mm and integrated sliding distance of 9.0 m, which corresponds to 2.25×10^3 cycles.

Optical microscopy and scanning electron microscopy (SEM) analyses were performed in the wear grooves, in order to observe scratch morphology.

Results and discussion

Structural characterization

X-ray diffraction patterns (data not shown) of untreated AISI 304 and AISI 316L samples present a typical austenitic structure, with peaks at 43.62, 50.837, and 74.772° (JCPDS card: 33-0397). Lattice parameters were $a = 3.5918(1)$ Å and $a = 3.5823(2)$ Å for untreated AISI 304 and AISI 316L, respectively. Due to mechanical polishing, untreated samples present small amount of martensitic α' phase ($a = 2.8729(4)$ Å) at 44.686° (JCPDS card: 35-1375). By increasing the working temperatures, martensitic α' amounts diminish, as a result of surface stress reduction.

Figure 1 shows XRD patterns between 35 and 75° of nitrocarburized samples at different temperatures. AISI 304 (Fig. 1a) and AISI 316L (Fig. 1b) samples, nitrocarburized at 400 °C, show expanded nitrogen austenite (γ_N) and γ'-Fe_4N nitride, with the latter being predominant. In both compositions a small amount of expanded carbon austenite (γ_C) is also observed at 42.76°. Expanded austenitic structures (γ_N and γ_C) were identified by comparing to the literature data [26]. Reportedly, expanded austenite presents various structures: (a) mixed fcc phase, when the grains have different lattice parameters, due to the increasing N concentrations; (b) tetragonal or triclinic; (c) fcc phase, with a high concentration of stacking faults. In a recent study about the crystallographic structure of expanded austenite, Fewell and Priest [27], using synchrotron radiation, reported the difficulty in indexing high or low reflection orders for this expanded austenitic structure. However, its formation is unequivocal; the primitive cell is cubic-like, and its actual crystallographic structure is strongly dependent upon plasma-based processes.

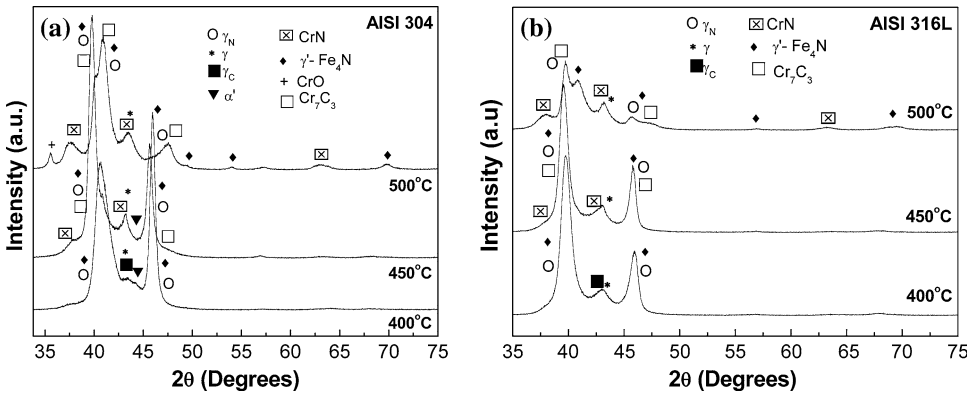

Fig. 1 X-ray diffraction patterns for **a** AISI 304 and **b** AISI 16L at different nitrocarburizing temperatures

At working temperatures of 450 and 500 °C, CrN and Cr_7C_3 phases are formed in both steels. A small amount of chromium oxide was observed in nitrocarburized AISI 304 at 500 °C. This finding was unexpected because the chamber pre-vacuum condition, before the plasma process, was approximately 10^{-3} Pa for all samples and working conditions. No diffraction peaks corresponding to Cr_2N phase and iron carbides were identified in the diffraction patterns.

Glancing-incidence X-ray analyses were carried out in order to obtain near surface structure information. Figure 2 shows the spectra for glancing incidences of $\alpha = 2°$ and 5° for samples of nitrocarburized AISI 304. This figure reveals the presence of a very complex mixture of different precipitate stoichiometries, including nitrides and carbides. The presence of carbides at near surface regions is congruent with previous findings [15–17], in which, by means of ion beam analysis, carbon was identified at this region. At the temperature of 500 °C, diffraction patterns have lower intensity than at lesser temperatures. This may be attributed to the high roughness observed in this sample that produces Bragg's diffuse reflections. The above-said occurrence limits analysis at modified near surface regions when roughness is high. However, at near surface regions the austenite phase is always present, which confirms that the formed precipitates are embedded in the austenitic matrix from the surface toward the bulk. Consequently, a full stoichiometric layer of nitrides and/or carbides at the surface is not present. The analysis of surface regions indicated chromium nitride at 400 °C (Fig. 2). According to literature [19], CrN formation is possible at near surface regions at this temperature.

Crystalline structures of different phases were refined using Rietveld's method. For all refinements the R_{wp} (%) values (weighted profile residual) were lower than 11%, which indicates the accordance between experimental data and fitting. Figure 3 shows the refinement (experimental and calculated X-ray diffraction patterns and the difference between them) of samples at 500 °C. Lattice parameters (Table 1) for the obtained phases were similar to those reported in the literature.

The lattice parameter of γ_N determined by refinement corresponds to $a = 3.7240(3)$ Å. According to literatures [28–30], two coexistent nitrogen-expanded austenite

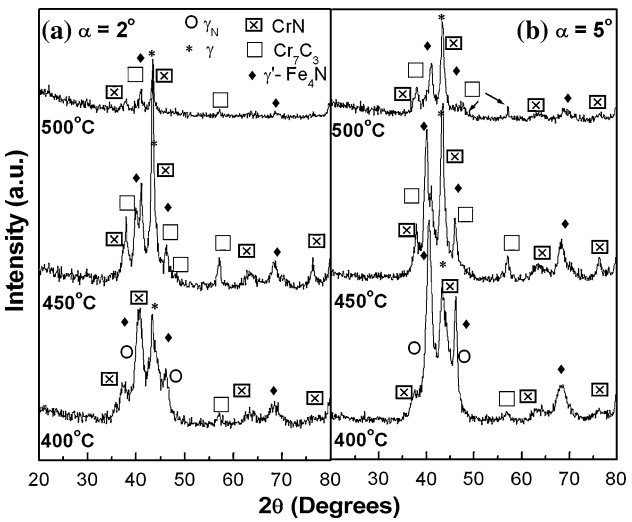

Fig. 2 Glancing X-ray diffraction patterns at $\alpha = 2°$ and $\alpha = 5°$ for AISI 304 nitrocarburized at 400, 450, and 500 °C

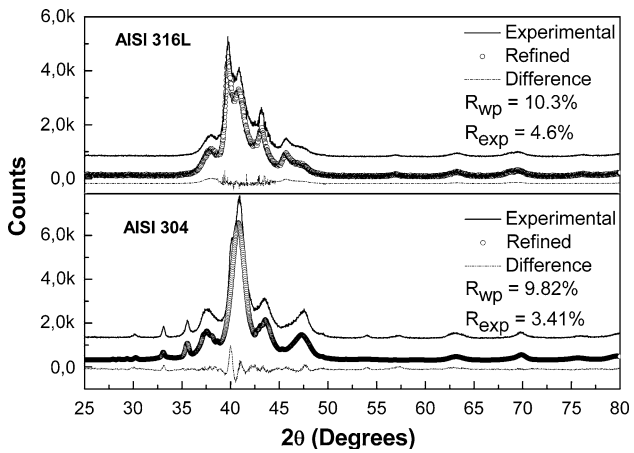

Fig. 3 Comparison between Rietveld's refinement of AISI 316L and AISI 304 nitrocarburized at 500 °C

Table 1 Phases, lattice parameters, space group, JCPDS cards, and (*hkl*) for nitrocarburized AISI 304 and 316L

Steel AISI	*T* (°C)	Phase	Lattice parameter (Å)	Space group	JCPDS ICSD	(*hkl*)
304	400	γ-austenite	3.5917(1)	*Fm-3m*	33-0397	(111)
		γ_N-austenite	3.7240(3)	*Fm-3m*	Ref. [21]	(111) (200)
		γ_C-austenite	3.6601(1)	*Fm-3m*	Ref. [21]	(111)
		α'-martensite	2.8674(3)	*Im-3m*	35-1375	(110)
		γ'-Fe_4N	3.7712(2)	*P-43m*	06-0627	(111) (200)
	450	γ-austenite	3.5821(4)	*Fm-3m*	33-0397	(111)
		γ_N-austenite	3.7263(1)	*Fm-3m*	Ref. [21]	(111) (200)
		α'-martensite	2.8672(4)	*Im-3m*	35-1375	(110)
		CrN	4.1214(3)	*Fm-3m*	11-0065	(111) (200)
		γ'-Fe_4N	3.7813(8)	*P-43m*	06-0627	(111) (200)
		Cr_7C_3	$a = 4.5385(2)$	*Pnma*	36-1482	(002) (321)
			$b = 7.1213(6)$		76799	
			$c = 12.1311(7)$			
	500	γ-austenite	3.5819(5)	*Fm-3m*	33-0397	(111)
		γ_N-austenite	3.7281(3)	*Fm-3m*	Ref. [21]	(111) (200)
		CrN	4.1411(3)	*Fm-3m*	11-0065	(111) (200) (220)
		CrO	8.4192(4)	*FE*	06-0532	(311)
		γ'-Fe_4N	3.7825(4)	*P-43m*	06-0627	(111) (200) (210) (211) (220)
		Cr_7C_3	$a = 4.5392(3)$	*Pnma*	36-1482	(002) (321)
			$b = 7.1211(8)$		76799	
			$c = 12.1331(3)$			
316L	400	γ-austenite	3.5822(4)	*Fm-3m*	33-0397	(111)
		γ_N-austenite	3.7236(3)	*Fm-3m*	Ref. [21]	(111) (200)
		γ_C-austenite	3.6524(5)	*Fm-3m*	Ref. [21]	(111)
		γ'-Fe_4N	3.7829(9)	*P-43m*	06-0627	(111) (200)
	450	γ-austenite	3.5825(7)	*Fm-3m*	33-0397	(111)
		γ_N-austenite	3.7260(1)	*Fm-3m*	Ref. [21]	(111) (200)
		CrN	4.1213(2)	*Fm-3m*	11-0065	(111) (200)
		γ'-Fe_4N	3.7825(3)	*P-43m*	06-0627	(111) (200)
		Cr_7C_3	$a = 4.5271(1)$	*Pnma*	36-1482	(002) (321)
			$b = 7.1210(3)$		76799	
			$c = 12.1314(1)$			
	500	γ-austenite	3.5823(5)	*Fm-3m*	33-0397	(111)
		γ_N-austenite	3.7279(4)	*Fm-3m*	Ref. [21]	(111) (200)
		γ'-Fe_4N	3.7822(4)	*P-43m*	06-0627	(111) (200) (210) (220)
		CrN	4.1214(3)	*Fm-3m*	11-0065	(111) (200) (220)
		Cr_7C_3	$a = 4.5274(3)$	*Pnma*	36-1482	(002) (321)
			$b = 7.1212(4)$		76799	
			$c = 12.1336(4)$			

structures, γ_{N1} and γ_{N2}, can be formed during nitriding at low temperatures ($\leq$400 °C), one rich in nitrogen and the other poor, respectively. In this situation, the lattice parameter of the expanded austenitic structure corresponds to the one richest in nitrogen content (γ_{N2}), without indication of the poorest one.

Structural characterizations, for both alloys, indicate a decrease in the relative amount of Cr_7C_3 carbides (M_7C_3) at the surface, by increasing the treatment temperature from 450 to 500 °C. Blawert et al. [4], Sun and Haruman [17], and Tsujikawa et al. [18] reported that nitrocarburizing produces the presence of two carbon concentration profiles: (a) one at near surface, and (b) other after the N profile. Besides this, by increasing nitrocarburizing time, the position of the second carbon peak goes to deeper regions, while the amount of the first one diminishes. The

authors attribute this to higher carbon diffusibility compared to that of nitrogen. Considering that nitrogen is trapped by chromium sites in austenitic steels [31], there is a possibility that nitrogen is more easily trapped in chromium sites than carbon is, thus, allowing C to diffuse to deeper regions. Glancing-incidence X-ray diffraction $\theta-2\theta$ suggests the presence of carbon precipitates at near surface and deeper regions, in agreement with the results reported by Tsujikawa et al. [18] and Blawert et al. [4] with respect to the presence of two carbon peaks.

Different phase stoichiometries can be formed by nitriding, carburizing, and nitrocarburizing ion beam processes on steel. These differences are attributed to the different working conditions (atmosphere composition, pressure, and temperature). Based on our diffraction patterns, the present nitrocarburizing process on AISI 304 and AISI 316L steels forms expanded austenite and γ'-Fe_4N phases at 400 °C. By increasing the temperature, CrN and Cr_7C_3 phases are formed in both steels; this presence of carbides and nitrides means Cr depletion.

Hardness

The hardness profiles, obtained by instrumented indentation, of untreated and 400 °C nitrocarburized samples are shown in Fig. 4. A similar surface hardness (~5 GPa) is observed for the untreated steels. The higher hardness at near surface is basically due to the presence of martensitic phase induced by mechanical polishing. At deeper regions, hardness is in agreement with bulk values for these steels. Large hardness dispersions are observed for samples treated at 400 °C. This fact is due to the effect of roughness and also to local differences related to hard grain dispersion. The lower "apparent hardness" at shallow depths for sample AISI 316L is an artifact attributed to its higher roughness when compared to AISI 304. Even in materials that present constant hardness in depth, but presenting a rough surface, there is an asymptotic behavior tending to the actual value at deeper tip penetrations [32]. Thus, the actual hardness value at depths of about 200 nm for this sample is higher than the measured value, which tends to be 13–14 GPa or higher. The near surface hardening of nitrocarburized samples is similar to nitriding processes in the same steels and different working temperatures [8, 9]. However, in this present case, hardness at a depth of 1 μm has higher values than for only nitrided AISI 304 at the same temperature.

Hardness profiles of samples treated at 450 and 500 °C were also measured by instrumented indentation. The results suggested a high hardness at near surface, but the strong artifacts induced by roughness made the actual hardness determination very difficult. In order to overcome this difficulty conventional Vickers hardness measurements were made considering that the hard layer is thick. Figure 5 shows hardness profiles as a function of the applied load for the different working conditions in both steels. The remarkable result is that the sample of AISI 316L, nitrocarburized at 500 °C, shows a hardness of ~17 GPa for loads up to 3 N. At a load of 3.0 N, tip penetration is about 3–4 μm. At this depth lower hardness values (<8 GPa) were reported [8, 9] for nitrided AISI 304. This implies that nitrocarburizing at 500 °C on AISI 316L is more effective than for AISI 304, in generating a plateau-like high hardness deep region. It is well known that plasma nitriding produces modified layers that are thicker at higher working temperatures. The layer thickness can be about 1 μm at low temperatures (300 °C), reaching tenths of a micrometer for higher temperatures [33]. According to Saha and Nix [34], the hardness of a hard layer on a soft substrate is influenced by the substrate if the indenter penetration depth exceeds

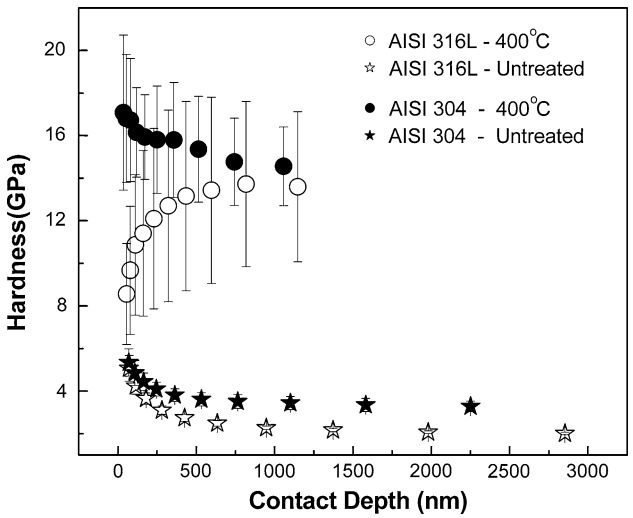

Fig. 4 Instrumented indentation hardness of untreated and 400 °C nitrocarburized AISI 304 and AISI 316L samples

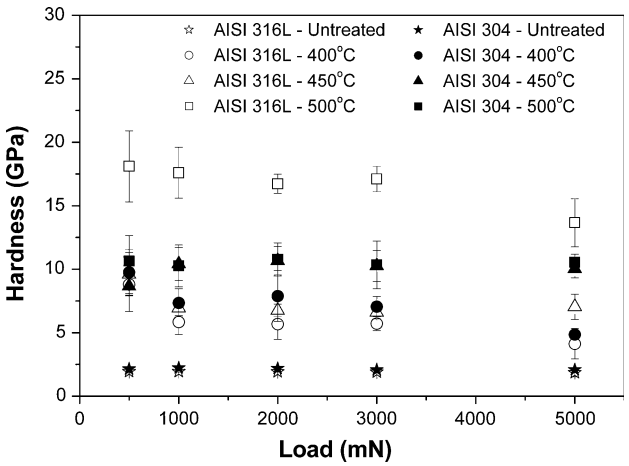

Fig. 5 Vickers hardness for untreated and nitrocarburized AISI 304 and AISI 316L samples

20% of the layer thickness. If the indenter penetration is more than 20% of the layer thickness, the measured hardness begins to decrease due to the influence of the soft substrate. Consequently, based on this assumption, it is possible to infer the thicknesses of a hard nitrocarburized layer. According to hardness profiles shown in Figs. 4 and 5, modified layers in samples treated at 500 °C are estimated to be thicker than 10 μm. On the other hand, layers of samples treated at 400 °C have lower thicknesses. The results show that AISI 316L enables the formation of a thicker hard layer than AISI 304 at 500 °C. The difference between both steels is with respect to Mo presence, which is about 1.9 wt% in AISI 316L. Consequently, it is possible that the presence of Mo facilitates N and C diffusion. However this statement needs additional investigations.

Tribological behavior

Reciprocating sliding

Both untreated samples present typical abrasive wear behavior [35, 36] for AISI 304. After a sliding distance of 3 m, the stationary regime value is reached for the friction coefficient. Friction coefficient profiles that shown in Fig. 6 for nitrocarburized AISI 316L samples show no significant differences with respect to the different working temperatures. This result is in contrast to that reported in the literature for nitriding only processes [8, 9]. The friction coefficients are lower than for nitrocarburizing, since the bulk stationary regime for only nitrided samples is not reached even at a sliding distance of 9 m. The samples of AISI 304, nitrocarburized at 450 and 500 °C, show a similar behavior when compared to AISI 316L at these temperatures. The only exception is for AISI 304 nitrocarburized at 400 °C, in which case, the bulk stationary regime is not reached even after a sliding distance of 9 m.

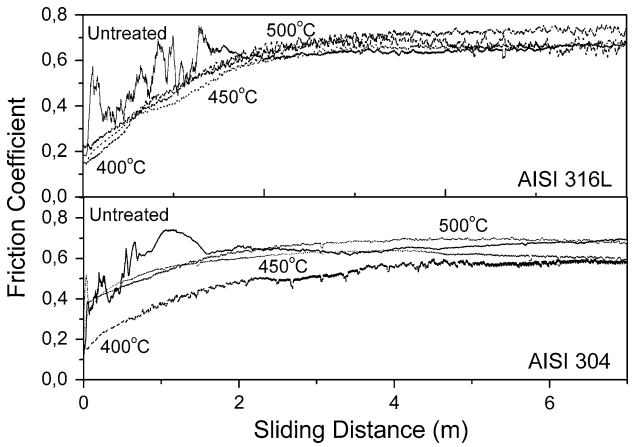

Fig. 6 Friction coefficient profiles as a function of sliding distance for untreated and nitrocarburized AISI 304 and AISI 316L samples

Figure 7 shows typical cross-sectional profiles at the mean track region of the groove produced after a sliding distance of 9 m for untreated samples and nitrocarburized samples at 400 and 500 °C. Untreated AISI 316L has a significantly deeper (~4000 nm) and larger groove (~400 nm) when compare to AISI 304 (~2000 and 300 nm, respectively). Despite the fact that the bulk hardnesses of both alloys are in the order of 2 to 3 GPa, the wear is much more intense on untreated AISI 316L than on untreated AISI 304.

Nitrocarburizing creates asperities that increase roughness, which rises with working temperature, as observed by profiles outside of the grooves shown in Fig. 7. Consequently, wear rates are difficult to obtain because roughness introduces artifacts to calculate the volume material that is worn out. However, a qualitative analysis of wear can be made based on groove profiles for different working conditions and steel samples. Hardness profiles (Fig. 5) reveal that the sample of AISI 316L at 500 °C has the highest hardness, around 16–17 GPa, up to a depth of 3 to 4 μm. For AISI 316L worked at 500 °C wear is restricted to mechanical deformation of asperities with "groove depths" of about 300 nm. In Fig. 7 it is possible to observe that the roughness degree at 500 °C is very high. A hard sphere of large radius pressed against a rough surface produces a mechanical deformation of the asperities. The combined effect of mechanical deformation and high hardness reduces wear, but this effect is difficult to quantify. Initially, wear occurs by smoothing the asperities through a reduction in their height. After that, hard precipitates are pulled out producing scars inside the groove by a three-body component mechanism (abrasive wear). The wear of sample AISI 304, at a temperature of 400 °C, is estimated to be as much as five times less than that of the untreated sample.

Nanoscratch

Figure 8 shows typical nanoscratch tip penetration profiles for samples worked at 500 °C and for untreated samples. Tip penetrations were performed with a ramping load from 0 to 400 mN. The three profiles for each sample correspond to original surface, scratch penetration, and post-scratch surface. The initial profile shows high roughness, under 500 °C working conditions, for both steels. Elastic recovery, evaluated from point to point after the scratch, is very similar in both alloys, in comparison to that of the untreated samples. This indicates that the elastic modulus should be similar for all samples, and the bulk elastic behavior is determinant in the recovery. A detailed analysis of scratch resistance for nitrocarburized samples is difficult to achieve due to high roughness level as observed in Figs. 7 and 8.

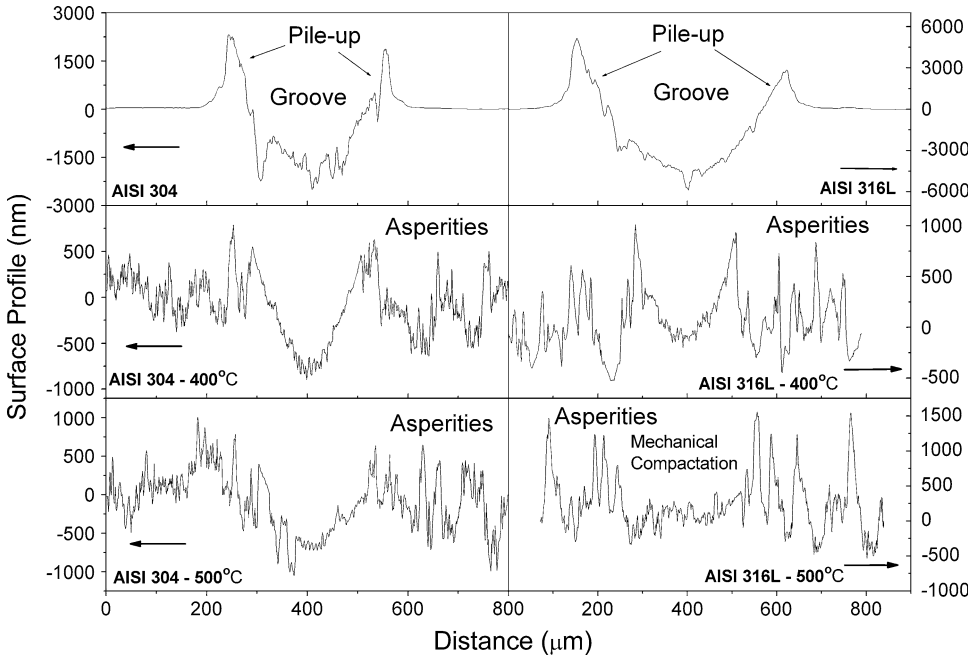

Fig. 7 Cross-sectional groove profiles for AISI 304 and AISI 316L, untreated and treated at 400 and 500 °C; groove, pile-up, and surface roughness are indicated

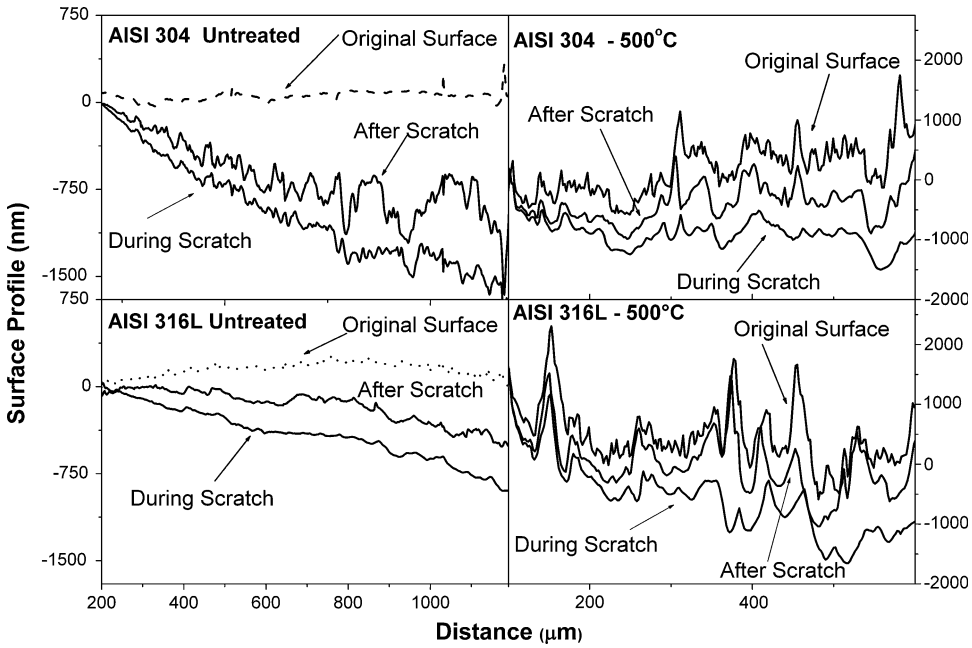

Fig. 8 Typical tip penetration profiles produced by nanoscratch tests, both for untreated AISI 304 and AISI 316L as well as for samples nitrocarburized at 500 °C; and profiles before, during, and after nanoscratch tests

Wear is reduced by the presence of nitrides and carbides in the surface region. The presence of asperities affects the contact area when a large radius sphere is used. Mechanical contact with asperities promotes their mechanical deformation. Roughness inside the groove is reduced, since the asperities are highly compacted. The energy necessary to deform mechanically the asperities with high hardness reduces the wear, but a quantitative evaluation of these effects is difficult to obtain.

Figure 9a shows a SEM image of three nanoscratch tests performed on the AISI 304 sample, nitrocarburized at 400 °C. During scratching the tip grooves grains of varying orientation, size, and nitride stoichiometry, which may induce large lateral forces and, consequently, tip deviance from a linear trajectory. A detail of this type of behavior is shown in Fig. 9b, where the presence of chipping at a groove's border is also indicated. The SEM image (Fig. 9c) of AISI 316L, nitrocarburized at the same temperature, also

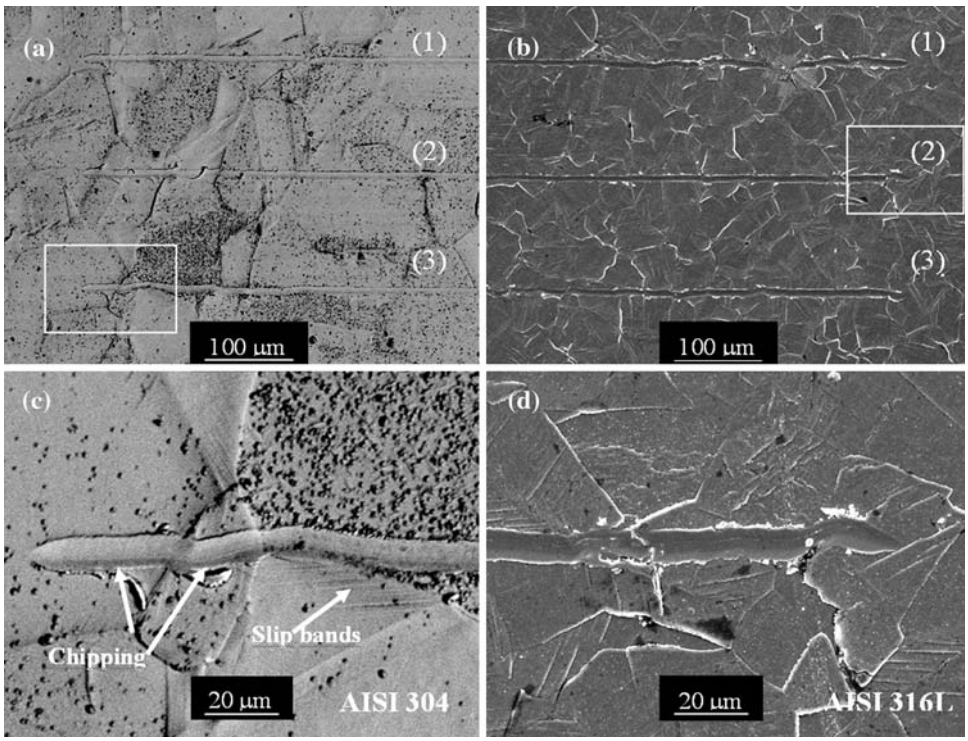

Fig. 9 **a** Nanoscratch images obtained by SEM of AISI 304, nitrocarburized at 400 °C; **b** detail of third nanoscratch test, where grain orientation affects scratch direction; **c** nanoscratch SEM image of AISI 316L, nitrocarburized at 400 °C; and **d** detail of second nanoscratch test

shows chipping at the groove's border (see details in Fig. 9d). It is also possible to observe in Fig. 9 a higher roughness degree for sample AISI 316L than for AISI 304.

Conclusions

Nitrocarburizing at low-carbon content on AISI 304 and AISI 316L steels produces a complex modified layer that includes the formation of carbide and nitride phases as embedded precipitates in the austenitic matrix. For working temperature of 400 °C, carbon and nitrogen-expanded austenitic (γ_N and γ_c) and γ'-Fe_4N are the predominant phases. Higher working temperatures create γ'-Fe_4N, Cr_7C_3, and CrN phases. The above-said formation of chromium nitrides and carbides is indicative of Cr depletion and probable reduction in corrosion resistance. Surface profilometry indicated that the roughness for AISI 316L is more intense when compare to AISI 304 at working temperatures higher than 400 °C.

Surface hardness for AISI 316L, treated at 500 °C, reaches $\sim$17 GPa, in a plateau-like profile, at depths $<\sim$10 μm. This may be an indicative of C and N diffusion being facilitated, by the presence of Mo in the alloy. However, the assertion of this statement requires future investigation. Nitrocarburizing processes yield thicker hard layers than solely nitriding, at equal working temperatures. In both alloys, wear mechanisms for high roughness corresponds to mechanical deformation of asperities. At a temperature of 400 °C, wear can be reduced by up to five times with respect to both untreated samples.

Acknowledgement We would like to acknowledge the Brazilian agency CNPq, for its financial support, and the Centro de Microscopia Eletrônica-UFPR.

References

1. Jones AM, Bull SJ (1996) Surf Coat Technol 83:269
2. Blawert C, Weisheit A, Mordike BL, Knoop FM (1996) Surf Coat Technol 85:15
3. Larisch B, Brusky U, Spies HJ (1999) Surf Coat Technol 116–119:205
4. Blawert C, Mordike BL, Collins GA, Short KT, Jirásková Y, Schneeweiss O, Perina V (2000) Surf Coat Technol 128–129:219
5. Hanninen H, Romu J, Ilola R, Tervo J, Laitinen A (2001) J Mater Process Technol 117:424
6. Tsujikawa M, Yamauchi N, Ueda N, Sone T, Hirose Y (2005) Surf Coat Technol 193:309
7. Sun Y (2005) J Mater Process Technol 168:189
8. Foerster CE, Serbena FC, da Silva SLR, Lepienski CM, Siqueira CJM, Ueda M (2007) Nucl Instrum Methods Phys Res B 257:732
9. Foerster CE, Souza JFP, Silva CA, Ueda M, Kuromoto NK, Serbena FC, Silva SLR, Lepienski CM (2007) Nucl Instrum Methods Phys Res B 257:727
10. Oddershede J, Christiansen TL, Stahl K, Somers MAJ (2008) J Mater Sci 43:5358. doi:10.1007/s10853-008-2791-y
11. da Silva LLG, Ueda M, Mello CB, Codaro EN, Lepienski CM (2008) J Mater Sci 43:5989. doi:10.1007/s10853-008-2768-x
12. Paternoster C, Fabrizi A, Cecchini R, El Mehtedi M, Choquet P (2008) J Mater Sci 43:3377. doi:10.1007/s10853-007-2392-1
13. Li CX, Dong H, Bell T (2006) J Mater Sci 41:6116. doi:10.1007/s10853-006-0484-y

14. Dasgupta A, Kuppusami P, Vijayalakshmi M, Raghunathan VS (2007) J Mater Sci 42:8447. doi:10.1007/s10853-007-1783-7
15. Chen FS, Chang CN (2003) Surf Coat Technol 173:9
16. Sun Y (2005) Mater Sci Eng A 404:124
17. Sun Y, Haruman E (2006) Vacuum 81:114
18. Tsujikawa M, Yoshida D, Yamauchi N, Ueda N, Sone T, Tanaka S (2005) Surf Coat Technol 200:507
19. Abd El-Rahamn AM, El-Hossary FM, Negm NZ, Prokert F, Richter E, Moeller W (2004) Nucl Instrum Methods Phys Res B 226:499
20. Abd El-Rahamn AM, El-Hossary FM, Fitz T, Negm NZ, Prokert F, Pham MT, Richter E, Moeller W (2004) Surf Coat Technol 183:268
21. Jenkins R, Fawcet TG, Smith DK, Visser JW, Morris MC, Frevel LK (1986) Powder Diffr 1:51
22. Rietveld HM (1967) Acta Crystallogr 22:151
23. Wiles DB, Young RA (1981) J Appl Crystallogr 14:149
24. Carvajal JR (2000) An introduction to the program FullProf. Lab Leon Brillouin, Saclay
25. Oliver WC, Pharr GM (1992) J Mater Res 7:1564
26. Blawert C, Kalvelage H, Mordike BL, Collins GA, Short KT, Jirásková Y, Schneeweiss O (2001) Surf Coat Technol 136:181
27. Fewell MP, Priest JM (2008) Surf Coat Technol 202:1802
28. Czerwiec T, Renevier N, Michel H (2000) Surf Coat Technol 131:267
29. Baranowska J, Franklin SE, Pelletier CGN (2005) Wear 259:432
30. Williamson DL, Davis JA, Wilbur PJ (1998) Surf Coat Technol 103–104:178
31. Parascandola S, Moeller W, Willianson DL (2000) Appl Phys Lett 67:2194
32. de Souza GB, Foerster CE, Silva SLR, Lepienski CM (2006) Mater Res 9:159
33. Alves C, Rodrigues JA (2000) Mat Sci Eng A 279:10
34. Saha R, Nix WD (2002) Acta Mater 5023:23
35. Zum Garh K-H (1987) Microstructure and wear of materials tribology series, vol 10. Elsevier, Amsterdam
36. Bushan B, Grupta BK (1991) Handbook of tribology coatings and surfaces treatments. McGraw-Hill, New York